

Multi-objective durability and layout design of fabric braided braking hose in cyclic motion

J.R. Cho^{*1} and Y.H. Kim²

¹Department of Naval Architecture and Ocean Engineering, Hongik University, Sejong 339-701, Korea

²Graduate School of Mechanical Engineering, Pusan National University, Busan 609-735, Korea

(Received November 03, 2016, Revised July 13, 2017, Accepted August 01, 2017)

Abstract. The fabric braided braking hose that delivers the driver's braking force to brake cylinder undergoes the large deformation cyclic motion according to the steering and bump/rebound motions of vehicle. The cyclic large deformation of braking hose may give rise to two critical problems: the interference with other adjacent vehicle parts and the micro cracking stemming from the fatigue damage accumulation. Hence, both the hose deformation and the fatigue damage become the critical issue in the design of braking hose. In this context, this paper introduces a multi-objective optimization method for minimizing the both quantities. The total length of hose and the helix angles of fabric braided composite layers are chosen for the design variables, and the maximum hose deformation and the critical fatigue life cycle are defined by the individual single objective functions. The trade-off between two single objective functions is made by introducing the weighting factors. The proposed optimization method is validated and the improvement of initial hose design is examined through the benchmark simulation. Furthermore, the dependence of optimum solutions on the weighting factors is also investigated.

Keywords: fabric braided rubber hose; cyclic motion; multi-objective optimization; durability and deformed layout; helix angle and hose length

1. Introduction

Fabric braided composite hoses are widely used for various industrial applications to convey high-pressure oil and gas. Braking hose used in automotive hydraulic braking system which delivers the driver's braking force to the brake cylinder without oil leakage becomes a representative example (Entwistle 1981). In braking hose, fabric braided composite layers are inserted between pure rubber layers to suppress the excessive radial expansion of rubber hose that is subjected to high internal braking pressure. In usual, two fabric braided layers are inserted into three pure rubber layers, that is, braking hose is in five-layered lamination. Fabric braided layer is woven with polyester cords in a specific micro structures that is composed of warp and fill tows. Due to the woven structure of fabric braided layers, the entire braking hose exhibits the remarkable anisotropic behavior to external loading (Li *et al.* 2011). And, the anisotropic behavior is influenced by the helix angle between warp and fill tows as well as the hose length and the geometric and material properties of base cords.

Meanwhile, braking hose undergoes a cyclic motion according to a combination of steering and bump/rebound motions of vehicle, and the anisotropically large deformation is accompanied by this cyclic motion. The hose cyclic motion is not unique but diverse depending on the hose cyclic path, hence the hose deformation configuration

is also dependent of the hose cyclic path. Here, the hose cyclic path is meant by the cyclic trajectory of hose movable end which is attached to the tire wheel of vehicle.

The cyclic motion-induced large deformation causes two critical problems; one is the interference between braking hose and other adjacent vehicle parts and the other is the accumulation of fatigue damage within braking hose. The frequent sliding contact of braking hose with other adjacent vehicle parts may cause wearing down of the outer rubber layer, while the fatigue damage accumulation may trigger the micro cracking (Kwack and Choi 2009, Malagi *et al.* 2015). Both the wearing down and the micro cracking not only weaken the structural strength of braking hose but also may lead to the function loss of braking hose owing to the oil leakage.

In this regard, the interference-free hose deformed layout and the suppression of fatigue damage accumulation (Ghazijahani *et al.* 2015) are currently a hot issue in the automotive industry, according to the worldwide intensification on the safety regulation of key automotive parts (Mayyas *et al.* 2012). However, the attempt to resolve the above mentioned two problems has been traditionally made by experiment that is not only cost- and time-consuming but also trial and error. The reliance on the experimental method was mainly owing to the difficulty in the geometric and material modeling of fabric braided layers in complex micro structure. One may simplify the fabric braided layers as isotropic solid because the modeling of warp and fill tows in micro structure is not only painstaking but also impractical (D'Amato 2001, Sun *et al.* 2003, Zhang and Xu 2013, Yang *et al.* 2015). However, such a simplified model cannot represent the inherent

*Corresponding author, Professor,
E-mail: jrcho@hongik.ac.kr

anisotropic out-of-plane deformation (Annie Peter *et al.* 2016) of fabric braided layers, and furthermore the effect of design parameters of fabric braided layers, such as the helix angle, cannot be taken into consideration.

To overcome the demerits of experimental approach and to effectively model the fabric braided layers, the application of the analytical and computational methods has been made by several investigators. Sugiyama and Otaki (1992) analytically predicted the hose deformed layout using a mathematical model that is constructed with the beam elements and particles and compared the analytical solution with the experiment. Keil *et al.* (2002) simulated the cyclic motion of braking hose by utilizing the CAD system and compared the hose deformed layout with the simulation using ADAMS. Cho *et al.* (2006) introduced a homogenization approach to model the fabric braided layers as a homogenized orthotropic solid and performed the large deformation and fatigue analyses using 3-D nonlinear finite element method.

Nevertheless, the design of interface-free and durable braking hose was not made by a reasonable approach but through trial and error. This implies that a systematic design method is highly desirable. In this context, the purpose of this paper is to introduce a multi-objective optimization method for the durability and layout design of fabric braided braking hose. The helix angles of braided layers and the total length of braking hose are chosen as the design variables, and the maximum hose deformation and the critical fatigue life cycle are defined as individual objective functions. Two single objective functions are approximated using the response surface method (RSM), and the weighted multi-objective optimization problem is solved by the progressive quadratic response surface modeling (PQRSM) (Nguyen *et al.* 2010). The proposed optimization method is validated and the improvement of initial hose design is confirmed through the benchmark simulation. In addition, the variation of optimum solutions to the trade-off between two single objective functions is investigated.

2. Problem description

2.1 Fabric braided braking hose in cyclic motion

A typical fabric braided braking hose used in the automotive hydraulic braking system is represented in Fig. 1(a), where one end is fixed to the main body of vehicle while the other end, called the movable end throughout this manuscript, is attached to the tire assembly using a strut. Hence, the hose movable end is to be moved along with the tire motion, and hence the entire braking hose is forced to be deformed. As shown in Fig. 1(b), the vehicle motion could be decomposed into the horizontal steering mode and the vertical bump/rebound mode. Here, the bump/rebound mode is resulted from the relative vertical motion of tire with respect to the vehicle at quick stop and start, or when the vehicle is running over cleats. The hose deformation is not only large and complicated but also repetitive, and furthermore the deformed braking hose may contact with other adjacent automotive parts and the hose durability

deteriorates in proportional to the repetition number of cyclic motion.

The path of hose movable end is not easy to identify because it is not unique but diverse according to a combination of the steering motion and the bump/rebound motion of vehicle. In fact, its realistic and exact identification would be possible only by either the motion measurement using the vision system or 3-D multi-body dynamics (MBD) simulation. However, even if possible, such measurement or MBD simulation requires the painstaking job for processing the numerous motion data. For this reason, the path is rather simply defined using nine extreme positions shown in Fig. 1(b) that are determined by the tensor product of three positions in the steering mode and three positions in the bump/rebound mode. The neutral position corresponds to the straight driving without bump and rebound, and the left and right positions indicate the maximum steering in the left and right directions. Meanwhile, the bump and rebound indicate the maximum compression and stretching of tire in the vertical direction with respect to the vehicle. Referring to Stalnaker and Turner (2002), the driving conditions are divided into nine modes and those are identical with the above-mentioned nine extreme positions. A number of paths could be defined by choosing three among nine extreme positions, but the significance of defined paths should be examined based on the real driving conditions of vehicle. The most representative is the horizontal path 2-1-3 which corresponds to the left-neutral-right handling in cruising.

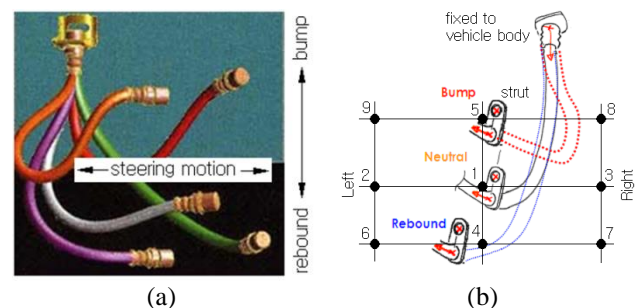


Fig. 1 Fabric braided braking hose: (a) steering and bump/rebound motions and (b) nine extreme positions of hose movable end

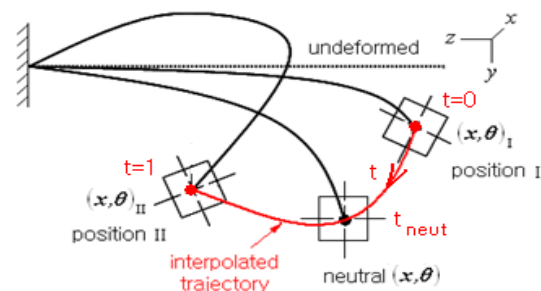


Fig. 2 Interpolation of the whole trajectory of hose cyclic path

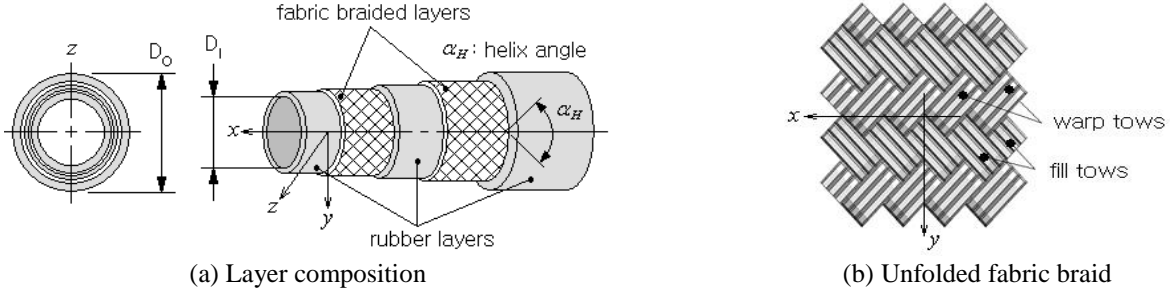


Fig. 3 Braided composite hose

The identification of nine extreme positions is much simpler and easier than that of the whole trajectory of path, and it is made by measuring three translation co-ordinates and three rotation angles of the strut (i.e., the hose movable end) with respect to the fixed co-ordinate system positioned at any reference point on the vehicle body. Once a path is defined in terms of three extreme positions, its whole trajectory could be approximated by the numerical interpolation method. For the sake of explanation, let us consider the path including the neutral position, as illustrated in Fig. 2. Three co-ordinates and three rotation angles of the hose movable end on the trajectory are interpolated using second-order polynomials, and the corresponding coefficients a_{ij} and b_{ij} are determined by solving the following two linear equation systems given by

$$\begin{cases} x(t) \\ y(t) \\ z(t) \end{cases} = \begin{bmatrix} a_{11} & a_{12} & a_{13} \\ a_{21} & a_{22} & a_{23} \\ a_{31} & a_{32} & a_{33} \end{bmatrix} \begin{bmatrix} 1 \\ t \\ t^2 \end{bmatrix}, \quad \begin{cases} \theta_x(t) \\ \theta_y(t) \\ \theta_z(t) \end{cases} = \begin{bmatrix} b_{11} & b_{12} & b_{13} \\ b_{21} & b_{22} & b_{23} \\ b_{31} & b_{32} & b_{33} \end{bmatrix} \begin{bmatrix} 1 \\ t \\ t^2 \end{bmatrix} \quad (1)$$

with the known values at three extreme positions and the parameter $t \in [0,1]$. Here, the values of parameter $t_{i,neut}$ for each co-ordinate parameter X_i at the neutral position are calculated by

$$t_{i,neut} = \frac{|X_{i,neut} - X_{i,I}|}{|X_{i,II} - X_{i,I}|}, \quad X_i = x, y, \dots, \theta_z \quad (2)$$

where the subscripts I and II indicate two positions shown in Fig. 2. The interpolated co-ordinates and rotation angles are used as the displacement boundary condition for the incremental large deformation analysis of braking hose.

2.2 Material models

Fig. 3(a) shows a five-layered braided composite hose composed of three rubber layers and two fabric braided layers, where the layers are assumed to be perfectly bonded. The unfold configuration of braided layer is represented in Fig. 3(b), where warp and fill tows are woven with the specific helix angle α_H . Each warp and fill tow are composed of three polyester cords, and the interfaces between warp and fill tows are also assumed to be perfectly bonded. We let M_B and d be the material properties and the diameter of base cords, and Cr be the total number of

bundles (i.e., warp and fill tows) within a pitch p . Then, the equivalent material properties \bar{M}_{FB} of fabric braided layers are characterized by

$$\bar{M}_{FB} = \bar{M}_{FB}(\alpha_H, M_B, d, p, Cr) \quad (3)$$

in terms of these parameters.

The microstructure of fabric braided layer is to be reoriented (Ivanov and Tabiel 2002) with the negligible strain during the deformation of braided composite hose up to the critical strain value. The reorientation causes the change of helix angle, which in turn results in the change of equivalent material properties of fabric braid. The reorientation phenomenon is a highly nonlinear problem because the change of helix angle cannot be known until the numerical simulation is completed. In fact, the strains of fabric braided layers are much smaller than those of rubber layers, so this phenomenon is ignored for the current study and the anisotropic behavior is modeled as a small-strain homogenized orthotropic solid, that is, the St. Venant-Kirchhoff model. With the setting of material co-ordinates shown in Fig. 3, two fabric braided layers are modeled as an orthotropic material with the constitutive relation (Daniel and Ishai 1994) given by

$$\begin{cases} \sigma_1 \\ \sigma_2 \\ \sigma_3 \\ \tau_{23} \\ \tau_{31} \\ \tau_{12} \end{cases} = \begin{bmatrix} S_{11} & S_{12} & S_{13} & 0 & 0 & 0 \\ S_{21} & S_{22} & S_{23} & 0 & 0 & 0 \\ S_{31} & S_{32} & S_{33} & 0 & 0 & 0 \\ 0 & 0 & 0 & S_{44} & 0 & 0 \\ 0 & 0 & 0 & 0 & S_{55} & 0 \\ 0 & 0 & 0 & 0 & 0 & S_{66} \end{bmatrix} \begin{cases} \varepsilon_1 \\ \varepsilon_2 \\ \varepsilon_3 \\ \gamma_{23} \\ \gamma_{31} \\ \gamma_{12} \end{cases} \quad (4)$$

with six diagonal terms defined by $S_{ii} = (1 - \nu_{jk\nu_{kj}})/E_j E_k \Delta$ and $S_{i+3i+3} = G_{ij}$. The other six off-diagonal terms are defined by

$$S_{ij} = \frac{\nu_{ji} + \nu_{ki} \nu_{jk}}{E_j E_k \Delta} \quad (i \rightarrow j \rightarrow k),$$

$$S_{kj} = \frac{\nu_{jk} + \nu_{ik} \nu_{ji}}{E_i E_j \Delta} \quad (k \rightarrow j \rightarrow i) \quad (5)$$

with $\Delta = (1 - \nu_{12}\nu_{21} - \nu_{23}\nu_{32} - \nu_{31}\nu_{13} - 2\nu_{12}\nu_{23}\nu_{31})/E_1 E_2 E_3$. Where, subscripts 1, 2 and 3 stand for x, y and z , respectively.

Meanwhile, the incompressible hyperelastic behavior of

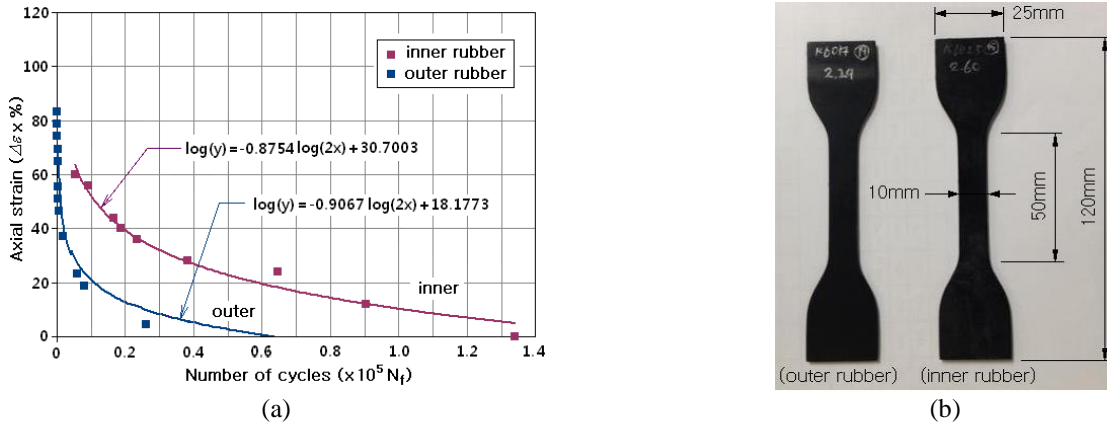


Fig. 4 (a) $\varepsilon - N$ curves of the inner and outer rubber layers and (b) rubber specimens for the fatigue test

three rubber layers is modeled by a four-term Mooney-Rivlin material model which is expressed by the strain energy density functional $W(I_1, I_2, I_3)$ defined by

$$W(I_1, I_2, I_3) = C_{10}(I_1 - 3) + C_{01}(I_2 - 3) + C_{20}(I_1 - 3)(I_2 - 3) + \frac{\kappa}{2}(I_3 - 1)^2 \quad (6)$$

In which, I_i are the invariants of Green-Lagrange strain tensor and C_{ij} are the material dependent Mooney-Rivlin constants. The incompressibility of rubber is enforced by the last term on the right hand side of Eq. (6), where the incompressibility enforcement becomes higher in proportional to the value of parameter κ . The Mooney-Rivlin constants which were determined by the uniaxial tension test of rubber specimen are given in Table A1 in appendix.

3. Durability and layout design of braking hose

3.1 Hose fatigue life and deformed layout

The braking hose is subjected to the cyclic motion with the presence of mean strain and stress, and the fatigue damage is to be accumulated within braking hose as the number of cyclic motion increases. For the fatigue life evaluation, only the outer and inner rubber layers are considered because both rubber layers play an important role in preventing the oil leakage. For the current study, the fatigue life cycle N_f of rubber layers is evaluated by the modified Morrow fatigue model (Smith *et al.* 1970) given by

$$\varepsilon_a = (K_f - \varepsilon_m)(2N_f)^b \quad (7)$$

which can consider the effect of mean strain ε_m of rubber hose on the fatigue damage. Two material-dependent parameters K_f and b in Eq. (7) were determined from $\varepsilon - N$ curves shown in Fig. 4(a) which were obtained by the uni-axial tension test using the rubber specimens shown in Fig. 4(b) under the displacement control (Cho *et al.* 2015). The fatigue strength exponents b and the fatigue

parameters K_f which were determined from $\varepsilon - N$ curves are as follows: -0.8754 and 30.7003 for the inner rubber layer and -0.9067 and 18.1773 for the outer rubber layer, respectively

For a given hose cyclic path, the fatigue life evaluation is performed node by node within rubber layers. Since the strains at each finite element node exhibit the complex time histories composed of a number of harmonic cycles, the Palmgren-Minor cumulative damage law (Palmgren 1924) given by

$$D_f = \frac{n_1}{(N_f)_1} + \dots + \frac{n_i}{(N_f)_i} + \dots + \frac{n_{N_s}}{(N_f)_{N_s}} \quad (8)$$

is employed to compute the total fatigue damage D_f . Here, N_s is the total number of distinct harmonic strain cycles, and n_i and $(N_f)_i$ are the repetition number and the fatigue life cycle of the i -th strain cycle. The repetition numbers n_i of each distinct harmonic strain cycle are counted by the rainflow cycle counting method, then finally the fatigue life cycle N_f (cycles) at each finite element node is calculated using $N_f = 1/D_f$.

Meanwhile, the sliding contact of the hose with other neighboring vehicle parts wears down the outer rubber layer, which may not only weaken the structural strength of hose but also trigger the fatal oil leakage. In this context, the prediction and design of hose deformed layout have been considered as important subjects. However, both have been traditionally made based on the trial and error experiment because the inherent anisotropic hose deformation cannot be accurately predicted by the conventional simple isotropic hose model. In fact, the layout prediction and design is a troublesome task because the hose deformed layout is dependent of cyclic path and continuously varying with the hose movement. Hence, the designer should evaluate a huge amount of hose deformation data at every moving stage for various cyclic paths to extract the characteristic deformation magnitude. Here, the characteristic deformation magnitude is usually meant by the maximum deformation.

In this regard, the numerical approach employing an

appropriate anisotropic hose model can successfully resolve the above-mentioned problems of the traditional experiment-based approach, because it can accurately and quickly obtain and evaluate the huge amount of hose deformation data. Nevertheless, the definition of characteristic deformation magnitude is still essential for the numerical approach. In fact, the choice of characteristic deformation magnitude depends on the design standard of car maker. Referring to Fig. 5, two principal maximum deformations, the maximum in-plane and out-of-plane deformations, would be usefully used to identify the deformed configuration of braking hose. Both of the maximum deformations are measured with respect to the straight line $a-a'$ which connects both ends of hose. The largest normal distance between the deformed hose and the straight line $a-a'$ always becomes the maximum in-plane deformation, while the other on the plane normal to the in-plane becomes the maximum out-of-plane deformation.

3.1 Formulation of multi-objective optimization problem

The fatigue damage and the deformed layout of fabric braided braking hose is influenced by several parameters such as the cyclic path, the hose length and diameter, the helix angle and the material properties of base cords. According to our preliminary parametric study to the cyclic path, it has been found that the horizontal path (i.e., path 2-1-3 in Fig. 1(b)) is critical in aspect of the fatigue damage and deformed layout. Based on this fact, the horizontal path is taken for the durability and layout design. Meanwhile, among other parameters affecting both performances, the hose length and the helix angle are importantly considered by the designers. Thus, in the current study, the design variable vector \mathbf{X} is defined by the total length L of braking hose and two helix angles $\alpha_{H.in}$ and $\alpha_{H.out}$ of inner and outer fabric braided layers such that

$$\mathbf{X} = \{\alpha_{H.in}, \alpha_{H.out}, L\} \quad (9)$$

The fatigue damage of braking hose is evaluated in terms of the critical fatigue life cycle N_f^{crit} of inner and outer rubber layers. On the other hand, the hose deformed layout is evaluated by the maximum in-plane deformation $\delta_{I,max}$ for the horizontal path. It is because the magnitude of maximum out-of-plane deformation $\delta_{O,max}$ is much smaller than the maximum in-plane deformation.

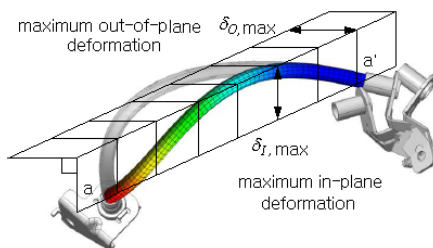


Fig. 5 Maximum in-plane and out-of-plane deformations

So, we choose $\delta_{I,max}$ and N_f^{crit} to define two objective functions $f_1(\mathbf{X})$ and $f_2(\mathbf{X})$ for the current study. However, in case of N_f^{crit} , some modification is required because the magnitude of N_f^{crit} is much larger than that of $\delta_{I,max}$ and N_f^{crit} should be maximized through the minimization process. For this reason, the second objective functions $f_2(\mathbf{X})$ are redefined by $1/\log(N_f^{crit})$, instead of N_f^{crit} . And, furthermore, two single objective functions are normalized as following

$$\bar{f}_I = \frac{f_I - f_I^{min}}{f_I^{max} - f_I^{min}}, \quad I = 1, 2 \quad (10)$$

With the setting of two normalized single objective functions \bar{f}_1 and \bar{f}_2 , the multi-objective function $F(\mathbf{X})$ is defined by

$$F(\mathbf{X}) = w_1 \bar{f}_1(\mathbf{X}) + c w_2 \bar{f}_2(\mathbf{X}) \quad (11)$$

with the weighting factor w_I and the scaling factor c . The weighting factor is introduced for trade-off between two normalized single objective functions, while the scaling factor which is defined by

$$c = \max|\bar{f}_1| / \max|\bar{f}_2| \quad (12)$$

is introduced to maintain the balance between the magnitudes of two single objective functions.

Then, the constrained multi-objective optimization problem for minimizing the deformed layout and maximizing the durability of fabric braided braking hose is formulated as follows

$$\text{Find } \mathbf{X} = \{X_i\}_{i=1}^{N_d}, \quad (13)$$

$$\text{Minimize } F(\mathbf{X}) \quad (14)$$

$$\text{Subject to: } \int_{\Omega^0} S_{ij}(\mathbf{u}) e_{ij}(\mathbf{v}) dV = \int_{\Omega^0} \rho^0 b_i dV + \int_{\partial\Omega_N^0} \hat{t}_i^0 v_i ds \quad (15)$$

$$X_{i,L} \leq X_i \leq X_{i,U}, \quad i = 1, \dots, N_d \quad (16)$$

with $N_d = 3$ and $X_{i,L}, X_{i,U}$ being the lower and upper limits of design variables. Here, $S_{ij}(\mathbf{u})$ and $e_{ij}(\mathbf{v})$ are the second Piola-Kirchhoff stresses and the Green-Lagrange strains, b_i the body force of braking hose, and \hat{t}_i^0 is the traction force converted to the initial hose configuration Ω^0 with the traction boundary $\partial\Omega_N^0$.

4. Numerical experiments

Fig. 6 represents a numerical example of five-layered braking hose with the initial length L of 245mm and the

outer diameter D_o of $10.5mm$. The thicknesses of five layers are as follows: $1.25, 0.30$ and $1.10mm$ for the outer, middle and inner rubber layers and $0.45mm$ for two fabric braided layers. The fabric braided layers are manufactured with PVA (poly vinyl alcohol) and the initial helix angles α_H , pitch p and C_r are as follows: $18.5mm, 24$ and 53° for the outer layer and $14.0mm, 20$ and 55° for the inner layer, meanwhile, three rubber layers are manufactured with EPDM (ethylene-propylene-diene-monomer). The homogenized orthotropic material properties of two fabric braided layers are given in Table A2 in appendix. The reader may refer to our previous paper (Cho *et al.* 2013) for the detailed material properties of PVA cords and the detailed derivation of homogenized orthotropic material properties by the superposition method incorporated with the unit-cell finite element analysis.

4.1 Meta models of two single-objective functions

The meta models of two normalized single objective functions $\bar{f}_1(\mathbf{X})$ of $\delta_{l,max}(\mathbf{X})$ and $\bar{f}_2(\mathbf{X})$ of $N_f^{crit}(\mathbf{X})$ are approximated by making use of the response surface method (RSM) and the full factorial design (FFD) (Altinkok 2016) with 27 experiment cases. The lower and upper limits of three design variables are set by $0^\circ \leq X_1, X_2 \leq 90^\circ$ and $230mm \leq X_3 \leq 260mm$, and the three levels for FFD are as follows: $35^\circ, 55^\circ$ and 75° for X_1 , $33^\circ, 53^\circ$ and 73° for X_2 , and $235, 245$ and $255mm$ for X_3 , respectively.

The approximated meta models of two normalized single objective functions are as follows

$$\begin{aligned} \bar{f}_1(\mathbf{X}) = & -23.93779 + 0.00293X_1 + 0.01691X_2 + 0.15212X_3 \\ & - 3.7 \times 10^{-5} X_1 X_2 - 4.060 \times 10^{-5} X_2 X_3 - 7.213 \times 10^{-7} X_3 X_1 \\ & - 1.704 \times 10^{-5} X_1^2 - 6.211 \times 10^{-5} X_2^2 - 0.00022X_3^2 \end{aligned} \quad (17)$$

$$\begin{aligned} \bar{f}_2(\mathbf{X}) = & 231.52948 - 0.03136X_1 - 0.36576X_2 - 1.75832X_3 \\ & - 3.334 \times 10^{-5} X_1 X_2 + 0.001624X_2 X_3 + 0.00037X_3 X_1 \\ & - 0.00056X_1^2 - 0.00042X_2^2 + 0.00329X_3^2 \end{aligned} \quad (18)$$

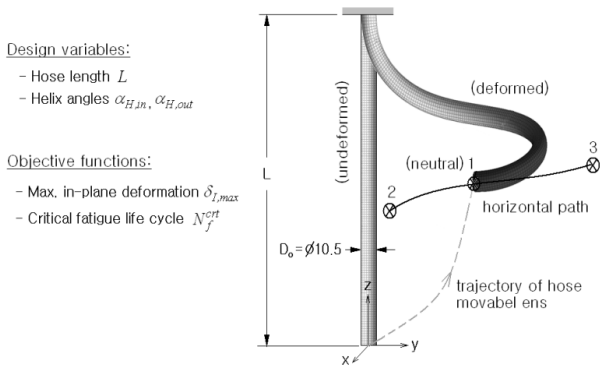
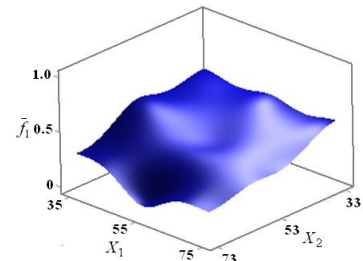


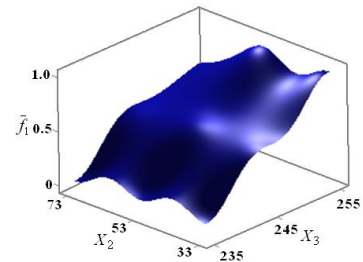
Fig. 6 A numerical example of braking hose

It was found that the R^2 values are 0.999 for \bar{f}_1 while 0.880 for \bar{f}_2 . The reason why the R^2 value of \bar{f}_2 is lower than one of \bar{f}_1 is because the fatigue life evaluation is more complex and its numerical accuracy is more sensitive to the associated parameters.

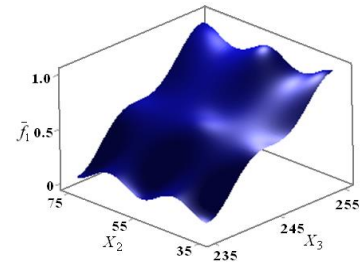
Fig. 7 represents the sensitivity of the normalized maximum in-plane deformation \bar{f}_1 to the design variables. First of all, it is found that the sensitivity of \bar{f}_1 is dominated by the hose length X_3 such that \bar{f}_1 uniformly increases in proportional to X_3 . On the other hand, the other two design variables X_1 and X_2 (i.e., the inner and outer helix angles) lead to the convex- and concave-type sensitivity. In case of the normalized critical fatigue life cycle \bar{f}_2 , its sensitivity to the design variables is quite different from that of \bar{f}_1 , as represented in Fig. 8. Reminding that \bar{f}_2 is defined by the reverse of the critical fatigue life cycle, it is found that the critical fatigue life cycle as a whole increases in proportional to the hose length X_3 . Meanwhile, to the helix angles X_1 and X_2 , the critical fatigue life cycle as a whole does not show the apparent variance, except for the its remarkable increase at high and low helix angles.



(a) With respect to X_1 and X_2



(b) With respect to X_2 and X_3



(c) With respect to X_1 and X_3

Fig. 7 sensitivity of the normalized fatigue life cycle \bar{f}_1 to the design variables

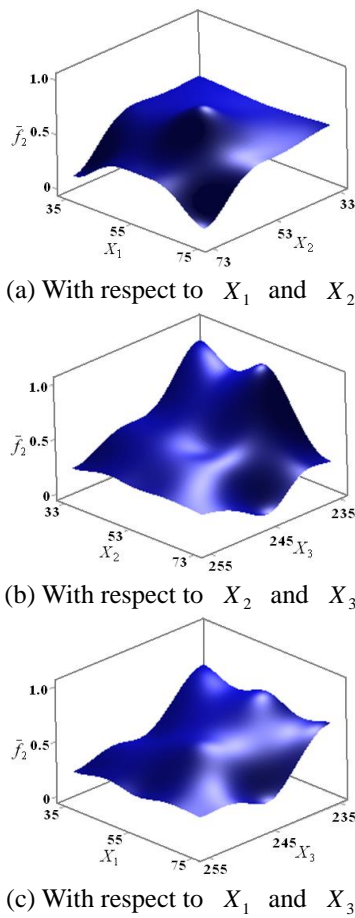


Fig. 8 sensitivity of the normalized fatigue life cycle \bar{f}_2 to the design variables

4.2 Optimization results

The multi-objective optimization was carried out using the progressive quadratic response surface modeling (PQRSM) (Nguyen *et al.* 2010), which is one of the SAO (sequential approximation optimization) algorithms, for constrained nonlinear optimization problems. The initial values of three design variables are set as follows: $\alpha_{H,in} = 55^\circ$, $\alpha_{H,out} = 53^\circ$ and $L = 245\text{mm}$. The iteration history of objective function $F(\mathbf{X})$ is represented in Fig. 9, where the objective function gradually decreases to near 0.14. The iteration terminates in twenty two iterations.

The optimization results are summarized in Table 1, where the results of initial hose model are also given for the comparison purpose. It is noted that the out-of-plane deformation $\delta_{O,max}$ and the peak equivalent values were obtained by the direct large deformation analysis using the initial and optimum design variables. It is found that two helix angles become larger while the hose length becomes shorter. The maximum in-plane deformation $\delta_{I,max}$ is reduced by almost 5mm (5.4% in the relative sense) and the critical fatigue life cycle N_f^{cr} is significantly improved near 4×10^5 cycles. And, it is also found that both the peak

equivalent strain and stress are reduced at the same time. However, the maximum out-of-plane (O-O-P) deformation $\delta_{O,max}$ is reversely increased, because it was not chosen as objective function.

Next, the optimization was performed for different combinations of weighting factors w_i of two single objective functions. Table 2 contains the optimization results for three different combinations of weighting factors. It is clearly found that the maximum in-plane deformation $\delta_{I,max}$ uniformly decreases as its weighting factor w_1 increases. This trend is also observed for the critical fatigue life cycle N_f^{cr} such that it monotonically increases as the second weighting factor w_2 increases. In case of the design variables, the optimum value of hose length decreases in proportional to w_1 but two helix angles are kept unchanged. Thus, it can be realized that two single objective functions are in the conflicting relation and their trade-off is dominated by the hose length, which is consistent with the sensitivities shown in Figs. 7 and 8 to the design variables. Meanwhile, it is also found that the maximum out-of-plane deformation $\delta_{O,max}$ uniformly decreases in proportional to the weighting factor w_1 , as in the maximum in-plane deformation. In addition, the peak equivalent strain and stress decrease with the increase of the second weighting factor w_2 , which is consistent with the fact that the critical fatigue life cycles increases in proportional to w_2 .

In order to evaluate the reliability of optimum solutions obtained using RSM meta models in Eqs. (17) and (18), both the maximum in-plane deformation $\delta_{I,max}$ and the critical fatigue life cycle N_f^{cr} were also obtained by the direct finite element analysis using the optimum design variables. Two single objective functions that were obtained using RSM meta models and the direct finite element analysis are compared in Table 3. It is found that the relative errors of the critical fatigue life cycle are much larger than those of the maximum in-plane deformation. The maximum relative difference is 8.29% that is occurred at the critical fatigue life cycle. In the second case (i.e., $w_1 = w_2 = 0.5$). By considering the fact that the accuracy of fatigue life evaluation is affected by many factors, it has been justified that the present numerical optimization method using RSM meta models provides the reliable optimum solutions.

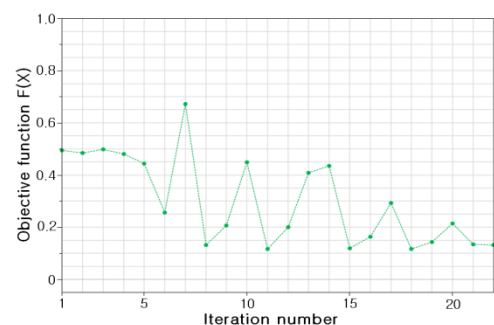


Fig. 9 Iteration history of the objective functions

Table 1 Comparison of two single objective functions between the initial and optimum models ($w_1 = w_2 = 0.5$)

Items	Design variables		Length $L(mm)$	Maximum deformation (mm)		Critical fatigue life cycle (Cycles)	Peak equivalent values	
	Helix angle (deg)			In-plane $\delta_{I,max}$	O-O-P $\delta_{O,max}$		Strain	Stress (MPa)
	$\alpha_{H,in}$	$\alpha_{H,out}$						
Initial	55	53	245.00	86.284	<u>11.673</u>	58,876	<u>0.296</u>	<u>1.883</u>
Optimum	75	73	239.54	81.582	<u>14.338</u>	447,217	<u>0.251</u>	<u>1.822</u>

O-O-P: Out-of-plane, (*): The values obtained by the direct finite element analysis

Table 2 Optimum results according to the change of weighting factors

Weighting factors (w_1, w_2)	Optimum design variables		Length $L(mm)$	Maximum deformation (mm)		Critical fatigue life cycle N_f^{crit} (cycles)	Peak equivalent values	
	Helix angle (deg)			In-plane $\delta_{I,max}$	O-O-P $\delta_{O,max}$		Strain	Stress (MPa)
	$\alpha_{H,in}$	$\alpha_{H,out}$						
(0.25, 0.75)	75	73	245.12	85.018	<u>14.961</u>	976,337	<u>0.208</u>	<u>1.524</u>
(0.5, 0.5)	75	73	239.54	81.582	<u>14.338</u>	447,217	<u>0.251</u>	<u>1.822</u>
(0.75, 0.25)	75	73	235.00	78.018	<u>14.303</u>	160,534	<u>0.299</u>	<u>2.143</u>

(*): The values obtained by the direct finite element analysis

Table 3 Comparison of the optimum results with the direct finite element analysis

Weighting factors (w_1, w_2)	Method	Objective functions	
		Maximum in-plane deformation $\delta_{I,max}$ (mm)	Critical fatigue life cycles N_f^{crit} (cycles)
(0.25, 0.75)	RSM	85.018 (+0.03%)	976,337 (+7.76%)
	FEM	84.989	905,947
(0.50, 0.50)	RSM	81.582 (+0.10%)	447,217 (+8.29%)
	FEM	81.499	412,991
(0.75, 0.25)	RSM	78.018 (-0.68%)	160,534 (-6.82%)
	FEM	78.557	172,283

(*): The relative differences of RSM with respect to FEM

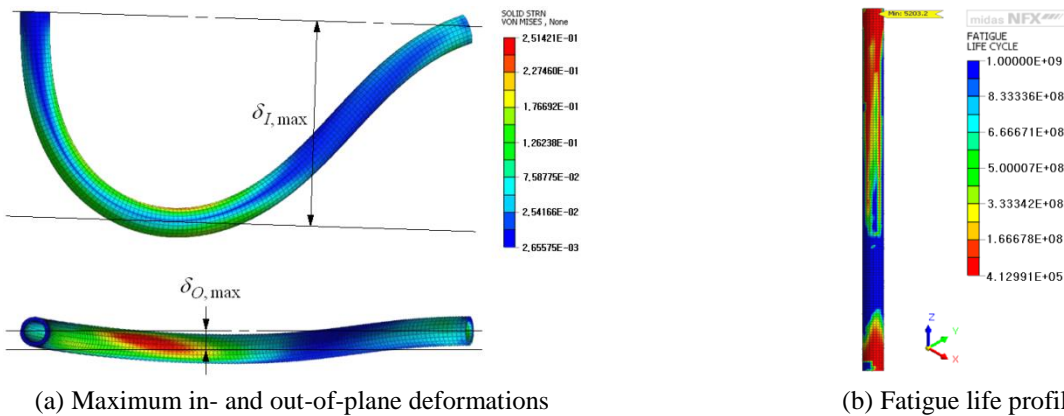


Fig. 10 Finite element analysis results obtained using the optimum design values ($w_1 = w_2 = 0.5$)

Fig. 10 represents the deformed layout and the fatigue life profile that were obtained by the finite element analysis using the optimum design variables. The deformation and fatigue analysis was carried out using a commercial software midas NFX (2011). The fixed end of braking hose is the left side in the deformed layout, while it is top side in the fatigue life profile. One can see the apparent out-of-plane deformation from the deformed layout owing to the anisotropy of fabric braided layers. Meanwhile, it is observed from the fatigue life profile that the fatigue damage is concentrated in the vicinity of two hose ends. It is because these two regions are in the relatively high state of combined bending, torsion and tensile stresses. The critical fatigue life cycle is occurred near the upper fixed end.

However, unfortunately the comparison of the maximum in-plane deformation and the critical fatigue life cycle between numerical and experiment was not made owing to the difficulty in changing the helix angle of braking hose in mass production and the difference of standards for judgment of the fatigue life cycle between numerical and experiment. But, in case of helix angles 55° and 53° , the reader may refer to our previous paper (Cho *et al.* 2013), where the deformed layout are compared through the twisting test of a U-shape braking hose.

5. Conclusions

In this paper, a multi-objective optimization method has been introduced for the deformed layout design of high-durable fabric braided automotive braking hose. The maximum in-plane hose deformation and the critical fatigue life cycle were defined by the single objective functions and their meta models were approximated by the response surface method. The trade-off between two single objective functions was implemented by adjusting the weighting factors. Based on our preliminary study, the helix angles of two fabric braided layers and the hose length were selected as the design variables. The proposed optimization method and its reliability were validated and verified through the benchmark experiments. According to the optimization, the durability and the deformed layout of the initial hose model have been successfully and remarkably improved. The maximum in-plane deformation has been reduced by 5.4% and the critical fatigue life cycle has been increased by 4×10^5 cycles. And, it has been justified that the proposed method successfully implements the trade-off between two single objective functions. The maximum in-plane deformation uniformly decreases with the increase of its weighting factor, and the critical fatigue life cycle does also uniformly increase in proportional to its weighting factor. Meanwhile, from the comparison with the direct finite element analysis, the reliability of proposed optimization method using RSM meta models has been verified such that the maximum relative difference in the critical fatigue life cycle is 8.29%. However, the present method is limited to the multi-objective optimization problems in which the number of single-objective functions is two.

Acknowledgements

This work was supported by 2017 Hongik University Research Fund. This research was supported by Basic Science Research Program through the National Research Foundation of Korea (NRF) funded by the Ministry of Education (Grant No. NRF-2014R1A1A2055820).

References

- Altinkok, N. (2016), "Application of the full factorial design to modeling of Al₂O₃/SiC particle reinforced al-matrix composites", *Steel Compos. Struct.*, **21**(6), 1327-1345.
- Annie Peter, G.J., Lakshmanan N. and Iyer, N.R. (2016), "Behavior of light weight sandwich panels under out of plane bending loading", *Steel Compos. Struct.*, **21**(4), 775-789.
- Cho, J.R., Jee, Y.B., Kim, W.J., Han, S.R. and Lee, S.B. (2013), "Homogenization of braided fabric composite for reliable large deformation analysis of reinforced rubber hose", *Composites: Part B*, **53**, 112-120.
- Cho, J.R., Song, J.I. and Choi, J.H. (2006), "Prediction of effective mechanical properties of reinforced braid by 3-D finite element analysis", *Key Eng. Mater.*, **306-308**, 799-804.
- Cho, J.R., Yoon, Y.H., Seo, C.W. and Kim, Y.G. (2015), "Fatigue life assessment of fabric braided composite rubber hose in complicated large deformation cyclic motion", *Finite Elem. Anal. Des.*, **100**, 65-76.
- D'Amato, E. (2001), "Finite element modeling of textile composites", *Compos. Struct.*, **54**(4), 467-475.
- Daniel, I.M. and Ishai, O. (1994), *Engineering Mechanics of Composite Materials*, Oxford University Press. New York.
- Entwistle, K.M. (1981), "The behavior of braided hydraulic hose reinforced with steel wires", *Int. J. Mech. Sci.*, **23**, 229-241.
- Ghazijahani, T.G., Jiao, H. and Holloway, D. (2015), "Fatigue tests of damaged tubes under flexural loading", *Steel Compos. Struct.*, **19**(1), 2015.
- Ivanov, I. and Tabiel, A. (2002), "Flexible woven fabric micromechanical material model with fiber reorientation", *Mech. Adv. Mater. Struct.*, **9**(1), 37-51.
- Keil, M., Rodriguez, J. and Hemmye, M. (2002), "Modeling and validation of large hydraulic hose deflections", *SAE Technical Paper 2002-01-2589*.
- Kwack, S.B. and Choi, N.S. (2009), "Micro-damage formation of a rubber hose assembly for automotive hydraulic brakes under a durability test", *Eng. Fail. Anal.*, **16**(4), 1262-1269.
- Li, D.S., Fang, D.N., Jiang, N. and Xuefeng, Y. (2011), "Finite element modeling of mechanical properties of 3D five-directional rectangular braided composites", *Composites Part B*, **42**(6), 1373-1385.
- Malagi, R.R. and Danawade, B.A. (2015), "Fatigue behavior of circular tube and wood filled circular hollow steel tube", *Steel Compos. Struct.*, **19**(3), 585-599.
- Mayyas, A., Qattawi, A., Omar, M. and Shan, D. (2012), "Design for sustainability in automotive industry: A comprehensive review", *Renew. Sust. Energ. Rev.*, **16**(4), 1845-1862.
- Midas IT (2011), *User's Manual of midas NFX*, Gyeonggi.
- Nguyen Xuan, H., Coulomb, J.L., Gerbaud, L. and Crebier, J.C. (2010), "Application of progressive quadratic response surface method for an oscillation problem optimization", *XI-th Int. Workshop Optimin. Inverse Prob. Electromagnetism*.
- Palgren, A. (1926), "Die lebensdauer von Kugellagern", *Zeitschr VDI*, **68**, 339-341.
- Smith, K.N., Watson, P. and Topper, T.H. (1970), "A stress-strain function for the fatigue of materials", *J. Mater.*, **5**, 767-778.

- Stalnaker, D.O. and Turner, J.L. (2002), "Vehicle and course characterization process for indoor tire wear simulation", *Tire Sci. Technol. TSTCA*, **30**(2), 100-121.
- Sugiyama, S. and Otaki, T. (1992), "Mathematical model for brake hose layout", *SAE Technical Paper 922123*.
- Sun, H., Di, S., Zhang, N., Pan, N. and Wu, C. (2003), "Micromechanics of braided composites via multivariable FEM", *Comput. Struct.*, **81**(20), 2021-2027.
- Yang, P., Dyke, S.V. and Elhajjar, F. (2015), "An investigation into the mechanics of fiber reinforced composite disc springs", *Steel Compos. Struct.*, **18**(3), 775-791.
- Zhang, C. and Xu, X. (2013), "Finite element analysis of 3D braided composites based on three unit-cell models", *Compos. Struct.*, **98**, 130-142.

CC

Appendix

Material properties of five layers and co-ordinates of three extreme positions

Table A1 Mooney-Rivlin constants and bulk moduli of three rubber layers

Rubber layer	C_{10}	C_{01}	C_{20}	κ
Inner	-1.86902	4.18478	0.41739	1,744.02150
Middle	0.15109	-0.14348	0.38478	7.84270
Outer	-2.46630	4.74565	0.48043	1,225.42264

Table A2 Homogenized orthotropic material properties of two fabric braided layers ($\alpha_{H,in} = 55^\circ$, $\alpha_{H,out} = 53^\circ$)

	Young's modulus			Poison's ratio			Shear Modulus		
	E_1	E_2	E_3	ν_{12}	ν_{23}	ν_{31}	G_{12}	G_{23}	G_{31}
Outer	819.2	733.1	1,128.4	0.05	0.16	0.16	14.6	6,490.8	8,241.5
Inner	915.3	801.0	1,547.1	0.03	0.15	0.18	17.8	6,832.7	8,816.2

Table A3 Co-ordinates and rotation angles of the hose movable end at three extreme positions

Positions	Center co-ordinates (mm)			Rotation angles (deg)		
	x	y	z	θ_x	θ_y	θ_z
1	-29.143	181.788	226.513	112.900	6.277	55.898
2	-34.787	152.647	224.121	107.916	-17.090	29.548
3	-37.039	206.245	232.331	112.454	28.343	78.412

List of nomenclature

\mathbf{X}	the design variable vector
X_I	individual design variables
$\alpha_{H,in}$	helix angle of the inner braided layer
$\alpha_{H,out}$	helix angle of the outer braided layer
L	total length of braking hose
$F(\mathbf{X})$	multi-objective function
$f_I(\mathbf{X})$	individual single-objective functions
$\bar{f}_I(\mathbf{X})$	normalized single-objective functions
$\delta_{I,max}$	maximum in-plane deformation
$\delta_{O,max}$	maximum out-of-plane deformation
N_f^{crit}	critical fatigue life cycle
w_I	weighting factors
c	normalization factor

